Methods 228 (2024) 55–64

Contents lists available at ScienceDirect

Methods

journal homepage: www.elsevier.com/locate/ymeth

Mobility of sodium ions in agarose gels probed through combined single- and triple-quantum NMR

Evgeny Nimerovsky [c,1], Daniel Sieme [1,c], Nasrollah Rezaei-Ghaleh [a,b,*]

[a] Heinrich Heine University Düsseldorf, Faculty of Mathematics and Natural Sciences, Institute of Physical Biology, Universitätsstraße 1 D-40225 Düsseldorf, Germany
[b] Institute of Biological Information Processing, IBI-7: Structural Biochemistry, Forschungszentrum Jülich D-52428 Jülich, Germany
[c] Department of NMR-based Structural Biology, Max Planck Institute for Multidisciplinary Sciences, Am Faßberg 11 D-37077 Göttingen, Germany

ARTICLE INFO

Keywords:
Condensates
Phase separation
Counterions
Hydrogels
quadrupolar NMR

ABSTRACT

Metal ions, including biologically prevalent sodium ions, can modulate electrostatic interactions frequently involved in the stability of condensed compartments in cells. Quantitative characterization of heterogeneous ion dynamics inside biomolecular condensates demands new experimental approaches. Here we develop a ^{23}Na NMR relaxation-based integrative approach to probe dynamics of sodium ions inside agarose gels as a model system. We exploit the electric quadrupole moment of spin-3/2 ^{23}Na nuclei and, through combination of single-quantum and triple-quantum-filtered ^{23}Na NMR relaxation methods, disentangle the relaxation contribution of different populations of sodium ions inside gels. Three populations of sodium ions are identified: a population with bi-exponential relaxation representing ions within the slow motion regime and two populations with mono-exponential relaxation but at different rates. Our study demonstrates the dynamical heterogeneity of sodium ions inside agarose gels and presents a new experimental approach for monitoring dynamics of sodium and other spin-3/2 ions (e.g. chloride) in condensed environments.

1. Introduction

Complex coacervation of proteins and ribonucleic acids has recently emerged as the key physicochemical mechanism underlying formation of membrane-less compartments inside cells [1]. The condensed phases formed through coacervation exhibit diverse material and biophysical properties ranging from liquid-like droplets to gel- and solid-like condensates [2]. Multivalent interactions, especially electrostatic interactions, are often the main driving force governing the formation of these condensates [3]. Various factors, such as charge-altering post-translational modifications and presence of metal ions, can modulate the network of electrostatic interactions among proteins and ribonucleic acids, hence regulate formation and dissolution of these condensates and tune their properties [4,5]. Besides, functional dynamics of biomolecules are coupled with motions of water molecules and ions within the highly crowded and frequently confined interior of these compartments [6]. Despite their potential importance in the function of these cellular compartments in health and disease [3], little is known about metal ion dynamics inside them. This is partly because of the experimental challenges to access heterogeneous ion dynamics inside biological condensates.

Here, we employ ^{23}Na NMR relaxation methods and investigate dynamics of biologically prevalent sodium ions dissolved in agarose gels as a model system. Agarose is a linear polymer of mainly uncharged disaccharide units, which is soluble in water at high temperatures but undergoes coil-to-double helix transition upon cooling and forms three-dimensional networks of helical aggregates as gels [7]. Sodium ion is a vital component of biological tissues, with intracellular concentrations ranging between 10–15 mM. The NMR active isotope of sodium is ^{23}Na, a spin-3/2 quadrupolar nucleus with natural abundance of almost 100 % and Larmor frequency of approximately 26 % of protons [8]. Dynamical behavior of sodium ions in agarose gels (or other porous materials) has been previously studied using single-quantum [9,10] or triple-quantum-filtered ^{23}Na NMR relaxation methods [11,12], respectively reporting the average dynamical behavior of “free” and “bound” or only that of “bound” sodium ions. Here, however, we exploit the quadrupolar

Abbreviations: TQF, Triple-Quantum-Filtered; IR, Inversion Recovery; SE, Spin-Echo; ILT, Inverse Laplace Transform.

* Corresponding author at: Heinrich Heine University Düsseldorf, Faculty of Mathematics and Natural Sciences, Institute of Physical Biology, Universitätsstraße 1 D-40225 Düsseldorf, Germany.
E-mail address: Nasrollah.Rezaie.Ghaleh@hhu.de (N. Rezaei-Ghaleh).

[1] These authors contributed equally to this work.

https://doi.org/10.1016/j.ymeth.2024.05.015
Received 11 March 2024; Received in revised form 17 May 2024; Accepted 20 May 2024
Available online 21 May 2024

relaxation of ^{23}Na nuclei and develop an integrative approach through combination of single-quantum and triple-quantum-filtered ^{23}Na NMR relaxation methods. The integrative approach so developed allows revealing the heterogeneous dynamics of sodium ions inside agarose gels.

2. Materials and methods

2.1. Preparation of agarose gels for NMR experiments

The agarose was acquired from Biozym (LE GeneticPure Agarose). Agarose gel samples were prepared as follows: the agarose powder was mixed with the corresponding amount of 100 mM NaCl (Sigma Aldrich) in deionized water to result in the given percentage gel (3–15 % agarose). The mixture was then subjected to a short period of microwave irradiation. When the agarose was fully solubilized, a 2–3 cm long sawed-off 5 mm NMR tube was inserted into the mixture to obtain a fragment suitable for inserting it into the NMR tube used for the actual experiments. For this, quartz glass 5 mm EPR tubes (Wilmad) were used after shortening them to a suitable length for NMR measurements. The transfer of gel samples was accomplished by pushing the sufficiently cooled gel fragment into the EPR tube that was subsequently submerged in a hot water bath close to the boiling point. This re-liquefied the gel inside the tube. By careful agitation of the tube, homogeneity of the samples was ensured during the heating process and air-bubbles were dissipated. The finished samples were left to cool at room temperature and sealed afterwards with a regular NMR tube cap and parafilm. The upper limit of 15 % for agarose concentration in our study was chosen for practical reasons, as it proved extremely difficult to prepare homogeneous agarose gels at higher concentrations inside NMR tubes following the above-described procedure.

2.2. NMR experiments

All NMR experiments were conducted at an Avance III HD Bruker spectrometer (Bruker, Germany) with a proton Larmor frequency of 400.13 MHz, equipped with a room-temperature triple resonance broadband (TBO) probe, at 298 K.

2.2.1. T_1 relaxation of water ^1H

The longitudinal spin–lattice (T_1) relaxation of water ^{1}H was measured through standard saturation-recovery experiments, as described before [13]. Briefly, after a long recycle delay, d_1, of 30 s, during which a continuous-wave (cw) irradiation at 100 Hz RF field strength applied on-resonance saturated water proton signal, there followed a block of variable duration (relaxation time, t between: 0.005 and 15.0 s). This allowed the T_1 relaxation-dependent recovery of the water proton signal and the intensity of recovered water proton signal was measured through a simple pulse-acquire experiment. To reduce the interference from radiation damping effects, the intensity of recovered signal was evaluated through integrated area intensity that equals the first point of FID, rather than peak height intensity, as recommended in ref. [14]. The signal intensity (I) *vs* relaxation time (t) data were then fitted to a single-exponential function,

$$I = a(1 - e^{-t/T_1}) \tag{1}$$

2.2.2. T_1 relaxation of water ^{17}O

The natural abundance ^{17}O experiments were performed at a Bruker spectrometer with ^{1}H Larmor frequency of 400.13 MHz, at which the inner broadband coil of the TBO probe was tuned and matched at the ^{17}O Larmor frequency of ~ 54.24 MHz. The T_1 relaxation of water ^{17}O was measured using the standard inversion-recovery experiment, as described before [15]. Briefly, after a sufficiently long total recycle delay, $d_1 + acq$, of ca. 0.66 s ensuring the complete recovery of Boltzmann magnetization for the quadrupolar ^{17}O nuclei, the ^{17}O magnetization was inverted using an on-resonance 180° pulse. Then, after a block of variable duration (0.25–30 ms), which led to the T_1 relaxation-dependent recovery of Boltzmann magnetization, the recovered signal intensity was measured through a simple pulse-acquire experiment. As expected under the so-called "extreme-narrowing" regime, the recovery of ^{17}O signal intensity (I) was nicely fit to the single-exponential recovery function,

$$I = a(1 - 2be^{-t/T_1}) \tag{2}$$

through which the T_1 relaxation times could be obtained. According to Redfield's relaxation theory, in the extreme narrowing regime where $\omega_0\tau_c \gg 1$ (ω_0, Larmor frequency, τ_c, rotational correlation time), the T_1 relaxation time of half-integer quadrupolar spins such as ^{17}O is identical to transverse spin–spin (T_2) relaxation time and is inversely proportional to τ_c, as in Eq. (3),

$$\frac{1}{T_1} = \frac{1}{T_2} = \frac{3\pi^2}{10}\left(\frac{2S+3}{S^2(2S-1)}\right)\chi^2\left(1+\frac{\eta^2}{3}\right)\tau_c \tag{3}$$

where I is the spin quantum number ($S = 5/2$ for ^{17}O), $\chi = e^2Qq_{zz}/h$ is the quadrupolar coupling constant (C_Q), Q is the quadrupole moment (Q = − 0.0256 barn for ^{17}O), and η is the asymmetry parameter representing the deviation of the electric field gradient (EFG) tensor q from axial symmetry [16].

2.2.3. ^1H and ^{23}Na NMR diffusion experiments

Diffusion coefficients (D) of water molecules and sodium ions were measured through ^{1}H- or ^{23}Na-based pulse-field-gradient (PFG)-NMR experiments, respectively. The standard stimulation-echo based pulse sequence of stebpgp1s was used for PFG-NMR diffusion measurements. The known diffusion coefficient of residual HDO in 99.8 % D_2O at 25 °C (1.900×10^{-9} $m^2.s^{-1}$) was used for gradient calibration. The magnetic field z-gradient-based intensity attenuation data were fitted to standard Stejskal-Tanner (ST) equation,

$$I = I_0\exp(-DQ) \tag{4}$$

with $Q = \gamma^2\delta^2(\Delta - \delta/3)g^2$, where γ is gyromagnetic ratio of the corresponding nucleus, g is magnetic field z-gradient strength and Δ and δ are respectively big and little diffusion delays [17]. As for the ^{1}H T_1 relaxation data, the intensity for this nucleus was determined by taking the integrated area intensity. For ^{23}Na, the peak height was used for the analysis. Depending on the nucleus type and experimental condition e.g. temperature, the big and little diffusion delays were adjusted to ensure sufficient gradient-dependent decay in signal intensities, while simultaneously minimizing relaxation-dependent intensity losses during diffusion delays.

2.2.4. Spectral parameters for ^{23}Na relaxation measurements

All experiments were acquired with the same acquisition parameters, except for the number of scans (NS), which for the sake of improving the signal-to-noise ratio, varied from sample to sample: 0.25 s for the recycle delay (d_1); 201.3077 ppm for the spectral width (SW) and 0.1922389 s for the acquisition time (AQ, t_{acq}). The Supplementary Table S1 summarizes the NS parameters used for each sample in various experiments. For each sample, the 90°-pulse length was optimized using a 180°-pulse experiment, during which the null signal was observed. The optimal 90°-pulse length varied between 23.6 μs and 24.0 μs for different samples. The Supplementary Fig. S3A–E depicts various NMR pulse sequences used for ^{23}Na NMR relaxation measurements.

2.2.4.1. T_1 And T_2 relaxation of ^{23}Na ions. The ^{23}Na NMR experiments were conducted at a Bruker spectrometer with ^{1}H Larmor frequency of 400.13 MHz, at which the inner broadband coil of the TBO probe was tuned and matched at ~ 105.84 MHz, corresponding to ^{23}Na Larmor frequency. The T_1 relaxation times of ^{23}Na were measured through

standard inversion-recovery (IR) experiments (Fig. S3B) [18]. For ^{23}Na T_1 experiments, relaxation delays between 0.25 and 240 ms were used. A total recycle delay ($d_1 + acq$) of ca. 0.67 s was used. The T_2 relaxation times of ^{23}Na ions were measured through standard Spin-Echo (SE) filtered experiments (Fig. S3C) [19]. Five different filtering delays (2Δ) of 0.2, 2, 4, 10 and 20 ms were used, and for each of them, the relaxation delay t_{mix} was varied between 0.1 and 140 ms.

2.2.4.2. Acquisition of triple quantum filtered ^{23}Na experiments. The NMR pulse sequences for transverse and longitudinal Triple Quantum Filtering (T_2-TQF and T_1-TQF) experiments are shown in Fig. S4D and E, respectively [20,21]. Briefly, in the T_2-TQF sequence (Fig. S3D), the first 90° pulse converts the z-magnetization to a rank-1 single-quantum coherence. Then, because of bi-exponential transverse relaxation during the relaxation delay τ, the density operator is evolved to a mixture of rank-1 and rank-3 single-quantum coherences. The 180° pulse at the middle of the relaxation delay only refocuses the possible phase (offset) evolution and does not affect relaxation. The 90° pulse at the end of relaxation delay then creates higher orders (double-quantum and triple-quantum) of the rank-3 coherence, without affecting its rank. The appropriate phase cycling of these pulses (and the receiver) then selects the created rank-3 triple-quantum coherence. Finally, the third 90° pulse reconverts the rank-3 triple-quantum coherence into a rank-3 single-quantum coherence. This coherence is not directly visible, but due to the bi-exponential relaxation process occurring during acquisition (t_{acq}), it is transformed to a mixture of rank-3 and rank-1 single-quantum coherence, which the latter can be directly detected. As a result, the NMR signal (Free Induction Decay, FID) starts at zero, builds-up and decays during t_{acq}. In the T_1-TQF sequence (Fig. S3E), a similar path of events occurs except that the initial 180° pulse creates a rank-1 zero-quantum coherence, which is subject to bi-exponential longitudinal relaxation during the relaxation delay τ, hence evolves to a mixture of rank-1 and rank-3 zero-quantum coherences during this period. In the T_2-TQF experiments, the relaxation delay τ was varied between 0.1 and 60 ms. In the T_1-TQF experiments, the relaxation delay τ was varied between 0.05 and 70 ms.

2.2.4.3. Numerical simulations. Numerical simulations were performed, solving the equation of motion (eqs. 6 and 18 in ref. [22]), where the static Hamiltonian consisted of the RF field Hamiltonian (if applied) and the fluctuating quadrupole Hamiltonian. The fluctuating quadrupolar interaction was described in the framework of the Redfield relaxation theory [22,23]. A set of tensor differential equations, as detailed in ref. [20], was derived, including 15 basis symmetric and antisymmetric tensor operators (excluding the identity operator) ranging from rank 1 to 3 (Eq. (1) in ref. [22]). These equations depended on the RF-field pulses (if applied) and three spectral density values (Eq. (9) below): J_0, J_1 and J_2 [20].

The simulated IR, filtered-SE and TQF experiments mimicked the Bruker experiments, consisting of the mixing (t_{mix}) and acquisition (t_{acq}) blocks, with the signal, $S(t_{mix}; t_{acq})$, depending on them. The Fast Fourier Transform (FFT, MATLAB R2019b) was applied on the detected dimension: $S(t_{mix}) = FFT\{S(t_{mix}; t_{acq})\}$. In simulations, the mixing time values were the same as in Bruker experiments (see the previous section). The detected parameters were 118.1 ppm for the spectral width (*SW*) and 0.2 s for the acquisition time (*AQ*, t_{acq}).

2.2.4.4. Analysis of ^{23}Na NMR data. As described above, for each sample, we collected ^{23}Na NMR relaxation data from Inversion Recovery (IR), filtered Spin Echo (SE), transverse Triple Quantum Filtered (T_2-TQF) and longitudinal Triple Quantum Filtered (T_1-TQF) experiments. Due to practical limitations, the T_1-TQF data could not be collected for the 9 % Agarose gel sample. All data were analyzed independently for each sample. The analysis of experimental data for each sample involved three steps:

Step 1. First, we analyzed IR and filtered-SE data, using the Inversion Laplace Transform (ILT) algorithm [24]. This analysis allowed obtaining T_1 and T_2 values, which were used in the subsequent steps as constraints. Further details regarding this analysis are available in the Supplementary Information, '*Inversion Laplace Transform*' section.

Step 2. Secondly, we analyzed data from T_2-TQF and T_1-TQF experiments. This analysis allowed obtaining the spectral densities, J_0, J_1 and J_2. [20] To achieve it, we compared the experimental and the analytical solutions of T_2-TQF (Eq. (5) and T_1-TQF (Eq. (6) experiments [22],

$$S_{T2-TQF}(\tau; t_{acq}) = \frac{9}{40}\left[e^{-(J_0+J_1)\tau} - e^{-(J_1+J_2)\tau}\right]\left[e^{-(J_0+J_1)t_{acq}} - e^{-(J_1+J_2)t_{acq}}\right] \quad (5)$$

$$S_{T1-TQF}(\tau; t_{acq}) = \frac{3}{10}\left[e^{-(2J_1)\tau} - e^{-(2J_2)\tau}\right]\left[e^{-(J_0+J_1)t_{acq}} - e^{-(J_1+J_2)t_{acq}}\right] \quad (6)$$

with the Fast Fourier Transform implemented on the acquisition time. Conventionally, in Eqs. (5) and (6), J_0, J_1 and J_2 values are replaced with two T_2 (T_{2s} and T_{2l}; $T_{2s} < T_{2l}$) and two T_1 (T_{1s} and T_{1l}; $T_{1s} < T_{1l}$) time constants as follows:

$$T_{2s} = (J_0 + J_1)^{-1}, T_{2l} = (J_1 + J_2)^{-1}; \quad (7)$$

$$T_{1s} = (2J_1)^{-1}, T_{1l} = (2J_2)^{-1}. \quad (8)$$

and J_0, J_1 and J_2, are as follows:

$$J_m(m\omega_0) = (2\pi)^2 \frac{3}{80}\frac{2S+3}{S^2(2S-1)}\left(\frac{\chi^2\tau_c}{1+(m\omega_0\tau_c)^2}\right) \quad (9)$$

for $m = 1, 2 or 3$, where τ_c is the correlation time, ω_0 is the Larmor frequency and χ is the root-mean-square coupling constant. To obtain J_0, J_1 and J_2 values we utilized all experimental points from T_2-TQF experiments and one specific point from the T_1-TQF experiments. This particular point corresponded to the mixing time at which the experimental T_1-TQF signal nearly reached its maximal intensity. This selection was due to comparatively low signal-to-noise ratio of the T_1-TQF signals in contrast to T_2-TQF signals. The next constraints were applied to narrow down the search space for J_0, J_1 and J_2 values:

i. The J_0 values were varied within the range of $[0.5 : 1.1]/[min(T_2)]$, where $min(T_2)$ represented the minimum value observed in the T_2 probability distribution from step 1 (ILT of SE experiments). This range was based on the Eq. (7) and the following relation:[22] $(T_{2s})^{-1} = J_0 + J_1 \gtrsim J_0$.
ii. The J_1 values were varied within the range of $[0.8/(2 \times max(T_1)) : 0.45/(min(T_2))]$, where $max(T_1)$ was the maximum value observed in the T_1 probability distribution from step 1 (ILT of IR experiments). This range was based on the Eq. (8).
iii. The J_2 values were varied within the range of $[0.05 : 1] \times J_1$, where J_1 was the value defined in (ii).

The best-fitted J_0, J_1, J_2 values were found by simultaneous implementation of the following conditions:

i. The minimization of the root-mean-square deviation was calculated as followed:

$rmsd = \sqrt{\frac{1}{n}\sum_{k=1}^{n}\left[S_{sim}(t_k) - S_{exp}(t_k)\right]^2}$, where n was number of the mixing time points; S_{sim} and S_{exp} represented the simulated and experimental T_2-TQF signals at t_k.

ii. The long component of the transverse relaxation, $T_{2l} = (J_1 + J_2)^{-1} < 1.05 \times max(T_1)$, where $max(T_1)$ represented the

maximum value observed in the T_1 probability distribution from step 1 (ILT of IR experiments).

iii. The position of the simulated S_{T1-TQF} signal with a maximal intensity did not deviate by more than two in absolute value from the index of the maximal value in the experimental S_{T1-TQF} array.

iv. $\left|\frac{\eta_{sim}-\eta_{exp}}{\eta_{exp}}\right| \leq \varepsilon_{max}$, where $\varepsilon_{max} = \begin{cases} 0.15 \text{for 9\% Agarose} \\ 0.10 \text{for else} \end{cases}$ and $\eta_X = \left[\frac{max(S_{T1-TQF})}{max(S_{T2-TQF})}\right]_X$. The value $max(S_{T2-TQF})$ represented the maximal signal intensity from either experimental (X = exp) or simulated (X = sim) T_2-TQF data. Similarly, $max(S_{T1-TQF})$ indicated the near-maximal signal intensity from either experimental (X = exp) or simulated (X = sim) T_1-TQF data. For the 9 % Agarose gel sample, ε_{max} was set to 0.15 since T_1-TQF was not collected for that sample. The η_{exp} was adjusted based on the average values of η_{exp} obtained from the 6 % and 12 % Agarose gel samples.

Further details regarding this analysis are available in Supplementary Information, the '*TQF data analysis*' section.

Step 3. Third, we reanalyzed the filtered-SE and IR experimental data, utilizing the previously obtained values (J_0, J_1, J_2) as constants in the numerical simulations.

In the numerical analysis, three populations of sodium ions in agarose gels had to be considered to contribute to the filtered-SE signals:

a. two populations (p_1, p_2) with mono-exponential relaxation rates: $(T_2)_1, (T_2)_2$.

b. one population (p_{3b}) with a bi-exponential relaxation rate, as obtained in the previous section.

Further explanation regarding this assumption is available in Supplementary Information, the '*filtered-Spin Echo (SE) data re-analysis" and "Inversion Recovery (IR) data re-analysis*' sections.

The best-fitted mono-exponential relaxation times $((T_2)_1, (T_2)_2)$ and relative populations $(p_1, p_2, p_{3b} = 1 - p_1 - p_2)$ were found by simultaneous implementation of the two following conditions (four variables in total):

i. The minimization of the root-mean-square deviation was calculated as followed:

$rmsd = \sum_{o=1}^{N} \frac{1}{N} \sqrt{\frac{1}{n}\sum_{k=1}^{n} \left[S_{sim}(\tau_o; t_k) - S_{exp}(\tau_o; t_k)\right]^2}$, where n was number of the points; S_{sim} and S_{exp} represented the simulated and experimental SE signals at t_k. τ_o represented the length of the filter and N the number of experiments with different lengths of the filter.

ii. $\left|\frac{\xi_{sim}-\xi_{exp}}{\xi_{exp}}\right| \leq 0.15$, where $\xi_X = \left[\frac{max(S_{T2-TQF})}{S_{90}}\right]_X$. The value $max(S_{T2-TQF})$ represented the maximal signal intensity from either experimental (X = exp) or simulated (X = sim) T2 −TQF data. S_{90} indicated the signal intensity from either experimental or simulated 90° experiment.

For IR experiments, we reanalyzed the IR experimental data, this time as a function of mixing time, utilizing the previously obtained values (J_0, J_1, J_2) and the relative populations (p_{1m}, p_{2m}, p_{3b}) as constants in the numerical simulations (see above). In all the experimental IR curves, the normalized first point, $\frac{IR(t_{mix}=0.05ms)}{IR(t_{mix}=240ms)}$, deviated from −1. To account for this in simulations, the flip angle of the inverse pulse was adjusted from 180° and recalculated for each experimental curve.

In the numerical analysis, a single mono-exponential longitudinal value, $(T_1)_m$, was obtained from comparison of the numerical and simulated IR signals. Upon comparing the experimental and simulated IR signals, we were not able to distinguish between the cases when $(T_1)_1 = (T_1)_2$ and when $(T_1)_1 < (T_1)_2$. Therefore, we considered only the first case: $(T_1)_m = (T_1)_1 = (T_1)_2$. Only one condition was applied to obtain the best fitted values for $(T_1)_1, (T_1)_2$:

i. Minimization of $rmsd = \sqrt{\frac{1}{n}\sum_{k=1}^{n} \left[S_{sim}(t_k) - S_{exp}(t_k)\right]^2}$, where n was number of the points; S_{sim} and S_{exp} represented the simulated and experimental IR signals at t_k.

3. Results

3.1. Restricted mobility of water molecules inside agarose gels

First, we utilized ^{1}H-based Pulse-Field-Gradient NMR (PFG-NMR) method [17] and measured the (translational) diffusion coefficient of water molecules in agarose gels with 3–15 % agarose concentrations. As expected, the diffusion coefficient of water molecules decreased in an agarose concentration-dependent manner (Fig. 1A and Supplementary Fig. S1), reflecting partial restriction in the translational mobility of water molecules at higher agarose concentrations. We then probed the rotational mobility of water molecules through ^{1}H T_1 relaxation measurements. The dominant T_1 relaxation mechanism for ^{1}H NMR of water is intra- and intermolecular ^{1}H–^{1}H dipolar coupling, which is modulated by reorientational mobility of water molecules with respect to the external magnetic field, and in the case of intermolecular dipolar interactions, also by translational mobility of water molecules affecting inter-proton distances. To avoid the artefacts caused by radiation damping, we used the standard saturation-recovery experiments for T_1 measurement of water (Fig. 1B) [14]. At 298 K, the rotational correlation time (τ_c) of water molecules is around 1.5 ps [15,25], which considering a proton Larmor frequency of 400.13 MHz, hence $\omega = 2.514 \times 10^9 rad.s^{-1}$ and $\omega\tau_c = 3.771 \times 10^{-3} \ll 1$, lies in the fast regime. In this regime of motion, an increase in τ_c caused by rotational mobility restriction is expected to reduce T_1. As shown in Fig. 1C, the ^{1}H T_1 of water exhibits an agarose concentration-dependent decrease in T_1, indicating the expected partial restriction in the rotational mobility of water molecules at gels with higher agarose concentrations.

To further investigate the rotational mobility of water molecules, we also measured the natural abundance ^{17}O T_1 of water in agarose gels at different agarose concentrations. The ^{17}O nucleus has a spin quantum number of 5/2 with a relatively large electric quadrupole moment (eQ), and the dominant relaxation mechanism for the ^{17}O nuclei of water molecules is the orientation-dependent interaction between this electric quadrupole moment and the electric field gradient present at the site of the ^{17}O nucleus. With τ_c of ~ 1.5 ps for water molecules at 298 K and ^{17}O Larmor frequency of 54.243 MHz, hence the $\omega\tau_c = 5.112 \times 10^{-4} \ll 1$, the rotational mobility of water molecules in the reference sample (100 mM NaCl in water) lies well within the fast "extreme-narrowing" regime, hence it is expected that the inherently tri-exponential relaxation of ^{17}O NMR signal collapses into a mono-exponential relaxation and the T_1 relaxation time is inversely proportional to τ_c [26]. In line with this expectation, the ^{17}O T_1 relaxation of the reference and agarose gel samples probed via standard inversion-recovery experiments followed a mono-exponential recovery (Fig. 1D), and the obtained ^{17}O T_1 relaxation time of the reference sample was 6.86 ± 0.05 ms, in excellent agreement with previous reports [15,27]. A similar mono-exponential recovery was observed in agarose gels with 3–15 % agarose concentration (Fig. 1D), indicating that the water mobility averaged between free and agarose-bound populations of water molecules remained within the extreme-narrowing regime. The obtained T_1 relaxation times however showed an agarose concentration-dependent decrease (Fig. 1E), reflecting increasing restriction in rotational mobility of water at gels with increasing agarose concentrations. Taken together, the ^{1}H PFG-NMR and ^{1}H and ^{17}O T_1 relaxation data demonstrated agarose concentration-dependent restriction in translational and rotational mobility of water molecules within agarose gels.

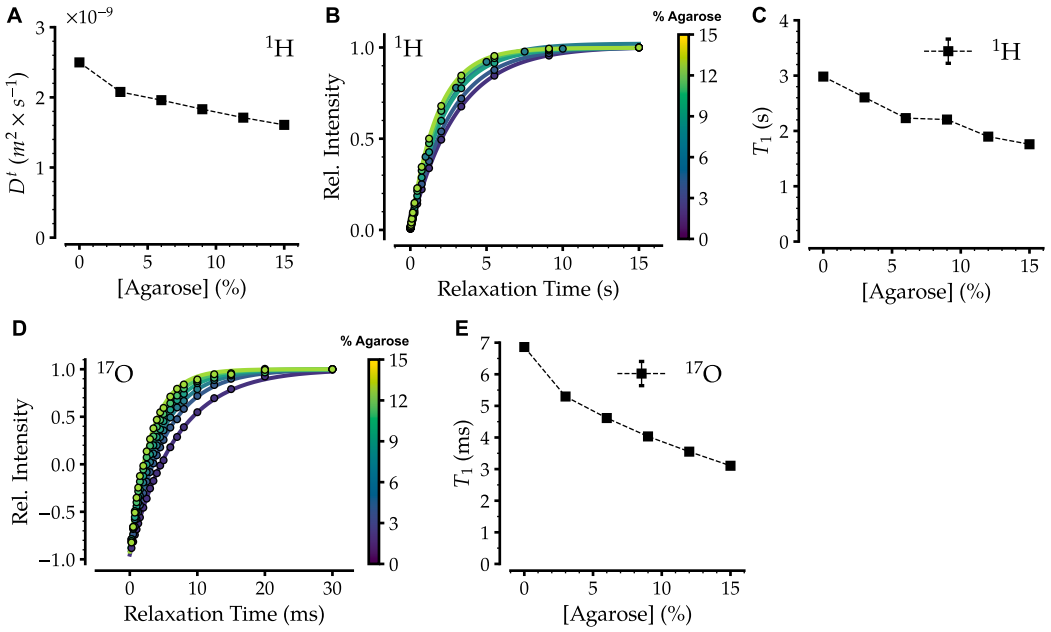

Fig. 1. Mobility of water molecules inside agarose gels. A. Diffusion coefficient of water molecules measured through ^{1}H-based PFG-NMR diffusion experiments. An agarose concentration-dependent decrease in (translational) mobility of water molecules is observed inside agarose gels. B,C. ^{1}H T_1 relaxation times measured through Saturation-Recovery experiments (B) are shown in C. An agarose concentration-dependent decrease in ^{1}H T_1 relaxation times is observed, indicating a reduction in rotational mobility of water molecules within the fast-motion regime inside agarose gels. D,E. ^{17}O T_1 relaxation times measured through natural abundance Inversion-Recovery experiments (D) are shown in E. The agarose concentration-dependent decrease in ^{17}O T_1 relaxation times is consistent with a reduction in rotational mobility of water molecules. The more pronounced changes in ^{17}O than ^{1}H T_1 suggests alterations in the average electric field gradients present at the site of ^{17}O nuclei in dependence of agarose concentration. Error bars represent fitting errors and are generally smaller than symbol size.

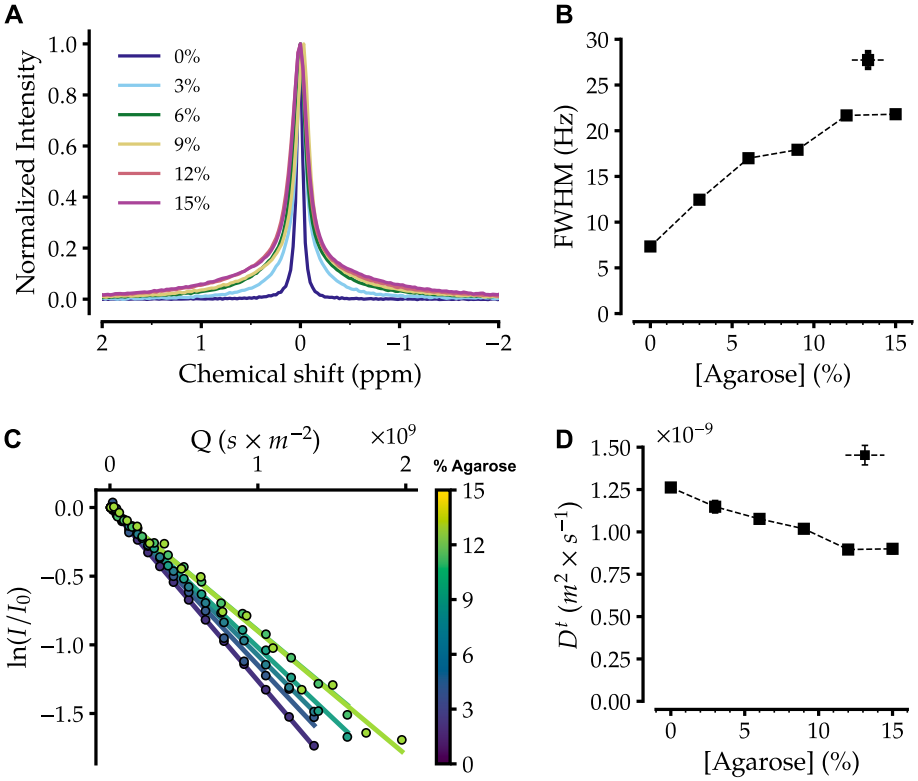

Fig. 2. Mobility of sodium ions inside agarose gels. A,B. 1D ^{23}Na NMR spectra measured at different agarose concentrations of agarose gels (A) shows agarose concentration-dependent increase in the linewidth (B, FWHM: Full Width Half Maximum) and gradual deviation from single-Lorentzian shape, consistent with reduction in rotational mobility of sodium ions. C,D. Diffusion coefficient of sodium ions measured through ^{23}Na-based PFG-NMR diffusion experiments. An agarose concentration-dependent decrease in (translational) mobility of sodium ions is observed inside agarose gels. Error bars represent fitting errors and are generally smaller than symbol size.

3.2. Retarded translational mobility of sodium ions inside agarose gels

Next, we utilized ^{23}Na NMR methods to probe mobility of sodium ions in agarose gels. The ^{23}Na nucleus has a spin quantum number of 3/2, hence possesses non-zero electric quadrupole moment and experiences anisotropic quadrupolar interaction with the local electric field gradient. The ^{23}Na nuclei have four energy levels with magnetic quantum numbers + 3/2, +1/2, −1/2, −3/2, with one central transition (CT, $+1/2 \leftrightarrow -1/2$) and one pair of satellite transitions (ST, $+1/2 \leftrightarrow +3/2$ and $-1/2 \leftrightarrow -3/2$). In isotropic media where the unrestricted rotational mobility of molecules averages out the anisotropic quadrupolar interactions, the four energy levels are equally spaced and the three transitions between them are degenerate. While the averaged out quadrupolar interaction does not affect the energy of transitions, it remains active for NMR relaxation and it is indeed typically the dominant relaxation mechanism for ^{23}Na and other quadrupolar nuclei in isotropic environments. The quadrupolar relaxation of the degenerate transitions of spin 3/2 nuclei is generally characterized by a bi-exponential process, unless the underlying molecular motions modulating quadrupolar interactions occur within the "extreme-narrowing" regime (for ^{23}Na nuclei with Larmor frequency of 105.819 MHz: $\tau_c \ll 1/\omega = 1.5ns$) where the two relaxation times converge and the relaxation process becomes mono-exponential [22,28]. In the reference sample where sodium ions are expected to move within the extreme-narrowing regime [29], the 1D ^{23}Na NMR signal had a single-Lorentzian line shape in accord with its mono-exponential transverse relaxation (Fig. 2A). In gels with 3–15 % agarose concentration, however, the ^{23}Na NMR signals appeared to deviate from single-Lorentzian line shape and contained a second Lorentzian component reflecting a partial contribution by sodium ions moving slower than τ_c of 1.5 ns. In line with the slower rotational mobility of sodium ions in agarose gels, an agarose concentration-dependent increase in the apparent line width of ^{23}Na signals was observed (Fig. 2B). In addition, the (average) diffusion coefficient of sodium ions obtained from PFG-NMR diffusion experiments revealed agarose concentration-dependent retardation in their translational mobility (Fig. 2C,D), in accord with previous reports [11].

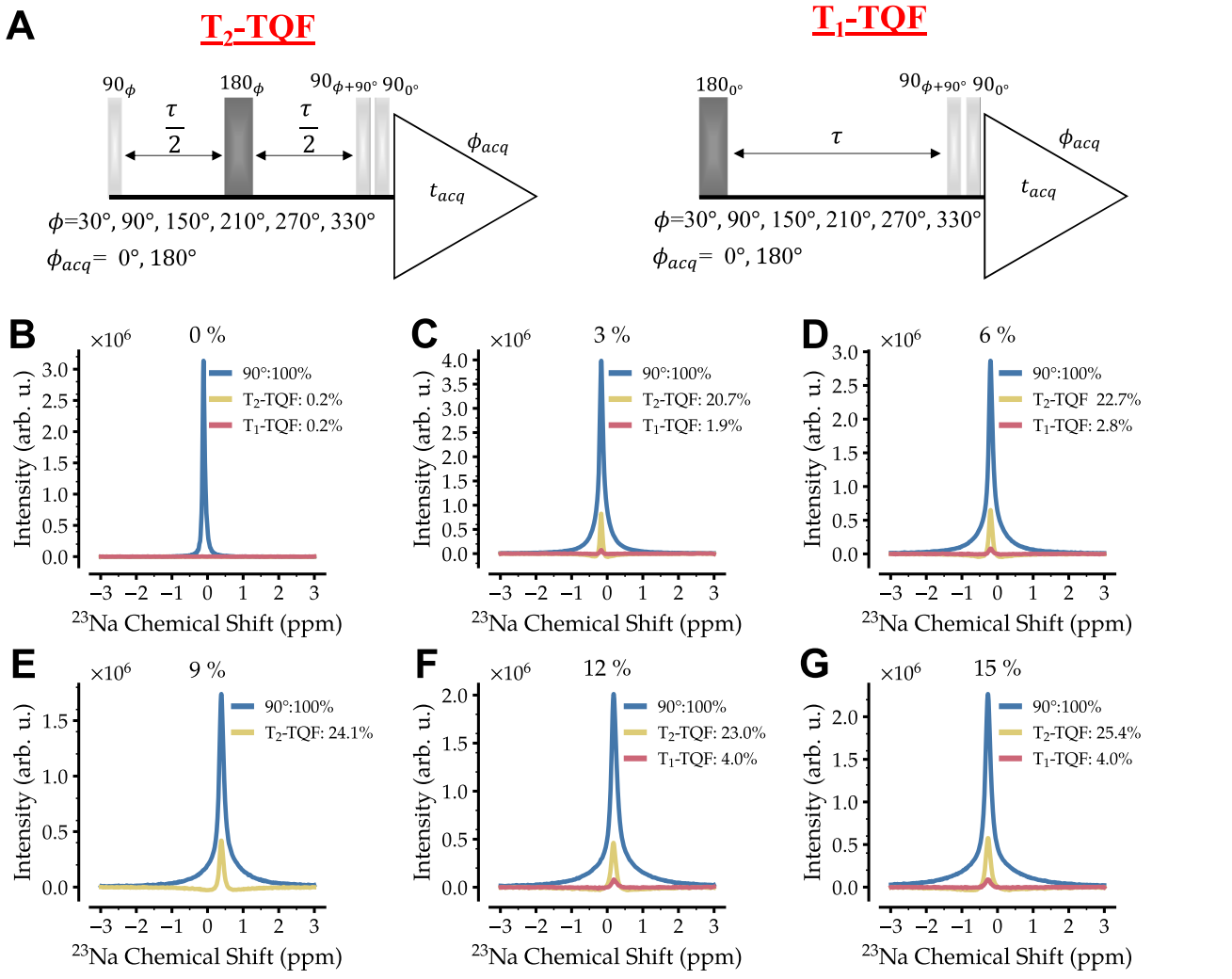

Fig. 3. Presence of sodium ions within slow motion regime inside agarose gels, detected through T_2- and T_1-Triple-Quantum-Filtered (TQF) ^{23}Na NMR spectra. A. Pulse sequences of the T_2- and T_1-TQF experiments. B-G. The T_2- (yellow) and T_1-TQF (red) ^{23}Na spectra of reference (B) and agarose gel samples (C-G) show the gradual emergence of T_1- and especially T_2-TQF ^{23}Na signals, reflecting the agarose concentration-dependent increase in the population of sodium ions within slow motion regime. The larger T_2-TQF ^{23}Na signal intensity is rooted in its dependence on the difference between J_0 and J_2, which is larger than the difference between J_1 and J_2 relevant for T_1-TQF signal (see the text for more details). The standard 1D ^{23}Na NMR spectra are shown in blue. Due to practical limitations, the T_1-TQF experiment was not measured for the 9 % agarose gel sample (panel E). (For interpretation of the references to colour in this figure legend, the reader is referred to the web version of this article.)

3.3. Restricted rotational mobility of sodium ions detected through ^{23}Na TQF NMR

Subsequently, we investigated the rotational mobility of sodium ions within agarose gels using ^{23}Na NMR relaxation experiments. Since the ^{23}Na NMR signal measured in agarose gels is an averaged signal over various sodium ion species moving within different motional regimes, as suggested above, we combined the standard Inversion-Recovery (IR) and filtered Spin-Echo (SE) experiments (Supplementary Fig. S3) with transverse and longitudinal Triple Quantum Filtered (T_2-TQF and T_1-TQF, respectively) experiments, which can directly access the sodium ion species moving in the slow-motion regime (Fig. 3A) [20,21].

The dynamics of spin 3/2 ^{23}Na nuclei in these TQF experiments can be best described through irreducible spherical tensor operators, by which the 4 × 4 density matrix can be represented as the sum of 16 operators T_{lm} with ranks $l = 0, 1, 2, 3$ and orders $m = -l, \cdots, +l$ [8,22]. Briefly, in T_2-TQF experiments (Fig. 3A), the first 90° RF pulse converts the z-magnetization (T_{10}) to a rank-1 single-quantum coherence ($T_{1\pm1}$). Then, during the relaxation delay τ, the quadrupolar relaxation in the isotropic environment converts the system to a mixture of odd-ranked single-quantum coherences, i.e. a mixture of rank-1 and rank-3 single-quantum coherences ($T_{1\pm1}$ and $T_{3\pm1}$). The mixture with even-ranked single-quantum coherence ($T_{2\pm1}$) is not allowed, unless the restricted rotational mobility in an anisotropic environment leads to a residual non-zero quadrupolar interaction [20]. Importantly, the efficient formation of rank-3 single-quantum coherence ($T_{3\pm1}$) occurs only if the difference between "short" (T_{2s}, depending on spectral densities J_0 and J_ω, henceforth J_0 and J_1) and "long" (T_{2l}, depending on spectral densities J_ω and $J_{2\omega}$, henceforth J_1 and J_2) transverse relaxation times is sizeable (equations (5) and (7). The second 90° RF pulse at the end of the relaxation delay τ then creates coherences with higher orders ($m = \pm2$, ±3 , double-quantum and triple-quantum) but with the same rank 3 ($T_{3\pm2}$ and $T_{3\pm3}$, respectively). The triple-quantum coherence can then be conveniently selected during acquisition using appropriate phase cycling for RF pulses and the receiver (see section 2.2.4.2 above for a detailed description of the TQF experiments). A similar process occurs during T_1-TQF experiments, except that during the relaxation delay τ, the rank-1 zero-quantum coherence (T_{10}) is mixed with rank-1 and rank-3 zero-quantum coherences (T_{10} and T_{30}) and the formation of rank-3 zero-quantum coherence (T_{30}) depends on the difference between "short" (T_{1s}, depending on spectral density J_1) and "long" (T_{1l}, depending on spectral density J_2) longitudinal relaxation times (equations (6) and (8) [30].

As expected, the reference sample did not show an appreciable ^{23}Na NMR signal in T_2- and T_1-TQF spectra (Fig. 3B, it was around 0.2 % for both T_2- and T_1-TQF spectra, when compared with the standard 1D NMR spectrum). It is because sodium ions move within fast extreme-narrowing regime in the reference sample and consequently the ^{23}Na NMR signal obeys a mono-exponential relaxation where the "short" and "long" components of relaxation are indistinguishable [22]. Conversely, in agarose gels, significant ^{23}Na NMR signals were observed in the T_2-TQF spectra, ranging from about 18 % to 25 % (relative to standard 1D NMR spectrum) in an almost agarose concentration-dependent manner (Fig. 3C-H). This indicates the significant presence of sodium ion species with slow motions and bi-exponential T_2 relaxation in agarose gels. Significant, albeit smaller, ^{23}Na NMR signals (ranging from about 2 % to 4 %) were also observed in the T_1-TQF spectra of agarose gels (Fig. 3C-H), further supporting the presence of slowly moving sodium ions inside them. The smaller size of T_1-TQF than T_2-TQF signals is rooted in their dependence on different spectral density terms: while the formation of T_1-TQF signal depends on the small difference between J_1 and J_2, that of T_2-TQF signal benefits the larger difference between J_0 and J_2 (equations (5)–(8) [22].

3.4. Combined single-quantum and TQF ^{23}Na NMR approach to detect populations of sodium ions

Next, we measured the longitudinal spin–lattice (T_1) and transverse spin–spin (T_2) relaxation times of ^{23}Na ions in reference sample and agarose gels through standard IR and filtered SE experiments (Fig. 4A and B). The relaxation data measured through these standard single-quantum NMR methods does not distinguish between different populations of sodium ions with fast or slow motions, instead represents an average relaxation behavior over those populations. On the other hand, the T_2-TQF and T_1-TQF relaxation data (Fig. 4C and D) directly probe the relaxation behavior of sodium ions in the slow-motion regime.

To disentangle the separate contribution of sodium ions with fast and slow motions to ^{23}Na relaxation, we therefore developed an integrative approach and analyzed the single-quantum IR and filtered SE data in combination with triple-quantum T_2-TQF and T_1-TQF data as follows (for details, see section 2.2.4.4 above and Supplementary Information): *(i)* the IR and filtered SE data were first analyzed using the Inverse Laplace Transform (ILT) algorithm [24]. The T_1 and T_2 distributions so obtained were used to define constraints for the subsequent step (Supplementary Figs. S4 and S5 and Table S2). *(ii)* Under the constraints defined in the previous step, the T_2-TQF and T_1-TQF data were analyzed and, through comparison between experimental data and analytic solutions (equations (5)–(8), the four relaxation times, $T_{2s}, T_{2l}, T_{1s}, T_{1l}$ and the three corresponding spectral densities J_0, J_1, J_2 were determined (Supplementary Figs. S6–S10 and Tables S3-S4). The obtained relaxation times report the bi-exponential relaxation behavior of the sodium ion species with slow motions and the spectral densities represent the characteristics of the underlying motions. Notably, the global fitting of T_2-TQF and T_1-TQF data was not achieved via a spectral density function with a standard single-Lorentzian shape. Instead, an excellent fit was obtained when a slightly modified single-Lorentzian spectral density function with one additional flexible parameter was used (see Supplementary Figs. S6-S10 and equations S1-S4). *(iii)* In the last step, the IR and filtered SE data were numerically simulated using the spectral densities J_0, J_1, J_2 and corresponding relaxation times $T_{2s}, T_{2l}, T_{1s}, T_{1l}$ for the bi-exponentially relaxing sodium ions species. When no other sodium ion species was taken into consideration, the agreement between numerically simulated and experimental filtered SE data was poor (Supplementary Fig. S11). Similarly, with addition of only one population of mono-exponentially relaxing species with adjustable population and relaxation times, the agreement between simulated and experimental data was less than satisfactory (Supplementary Fig. S12). However, with two populations of mono-exponentially relaxing sodium ion species with adjustable populations and relaxation times, an excellent agreement was achieved for both the filtered SE and IR data (Supplementary Figs. S13 and S14). The fitted values for populations and relaxation times of mono-exponentially relaxing species are included in Supplementary Table S5 for T_2 and Table S6 for T_1 relaxation times. Finally, the numerically simulated IR and filtered SE data based on the obtained fitting parameters were analyzed using the ILT algorithm. The obtained T_1 and T_2 distributions (Supplementary Figs. S15 and S16) were indistinguishable from the distributions derived from the same analysis of experimental data (Supplementary Figs. S5 and S6), supporting the self-consistency of our approach. The whole picture regarding populations of three sodium ion species inside agarose gels and their relaxation times in dependence of agarose gel concentration is summarized in Fig. 5 and supplementary Table S7 and discussed below.

4. Discussion

4.1. Three populations of sodium ions detected in agarose gels

Agarose is a linear uncharged polysaccharide, which can form three-dimensional networks as gels [7]. The average size of pores inside agarose gel varies with agarose concentration but is expected to be in the

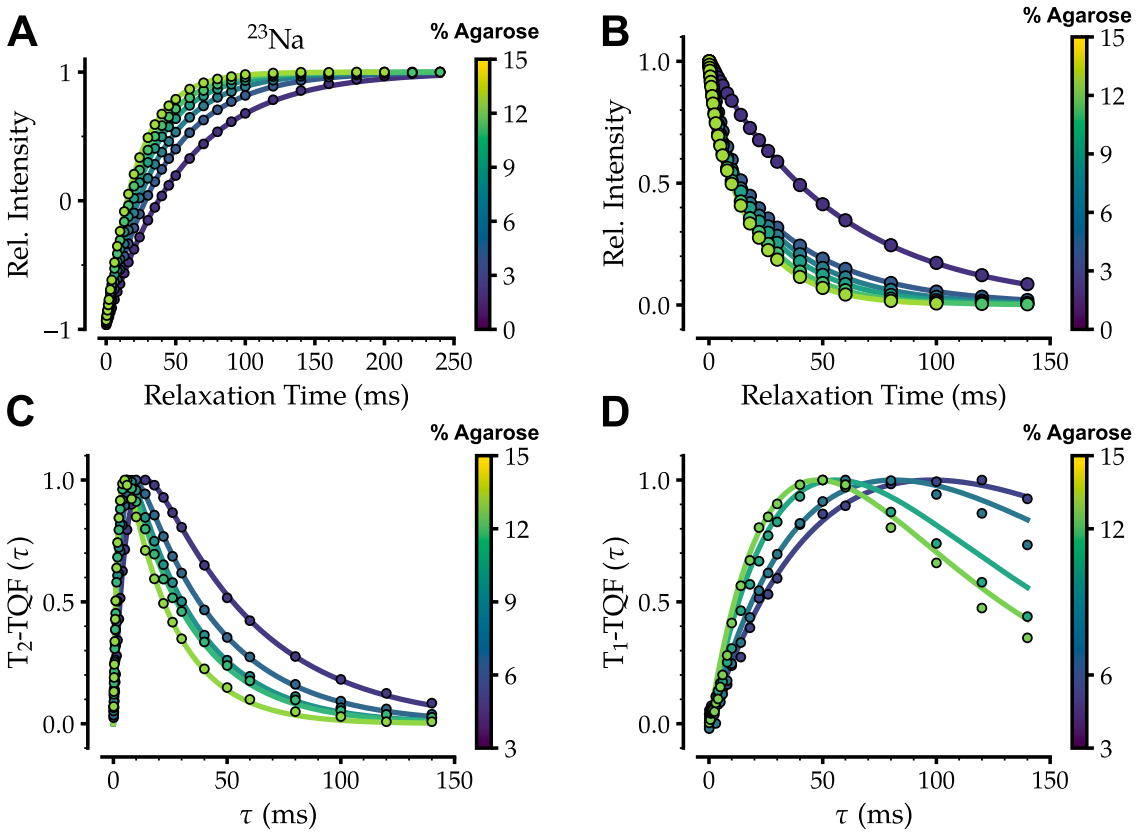

Fig. 4. Rotational mobility of sodium ions inside agarose gels monitored through ^{23}Na NMR relaxation experiments: A. Inversion-Recovery (IR), B. filtered Spin-Echo (SE), C. T_2-Triple-Quantum-Filtered (TQF), and D. T_1-TQF. The filtered SE data are shown for filter delay of 0.1 s as an example (B). In C and D, the x-axis (τ) represents relaxation delay, as shown in the related pulse sequences (see Fig. 3A). Due to practical limitations, the T_1-TQF measurement was not performed for the 9 % agarose gel sample.

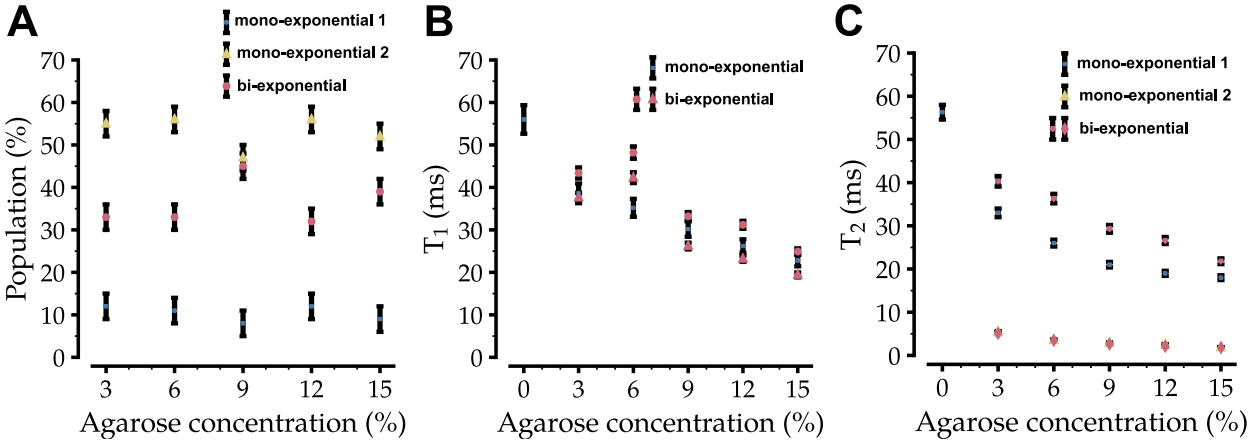

Fig. 5. Populations of sodium ions inside agarose gels (A) and their corresponding longitudinal, T_1 (B) and transverse, T_2 (C) relaxation times, derived from an integrated analysis of single-quantum (IR and filtered SE) and T_1- and T_2-Triple-Quantum-Filtered (TQF) ^{23}Na relaxation. Three populations are detected: one species with bi-exponential relaxation behavior (represented by two relaxation times, short T_{is} and long T_{il}, i: 1, 2) and two species with mono-exponential T_2 relaxation behavior. The two mono-exponentially relaxing species could not be distinguished based on their T_1 relaxation. No significant agarose concentration dependence in populations is observed (A), but the T_1 (B) and T_2 (C) relaxation times exhibit pronounced agarose concentration dependence. Error bars represent fitting errors.

range of tens to hundreds of nanometer at 3–15 % agarose concentration studied here [11]. The ^{1}H and ^{17}O NMR diffusion and T_1 relaxation data showed that water molecules experience significant restriction in the translational and rotational mobility of water molecules in an agarose-concentration-dependent manner (Fig. 1). The retarded mobility of water molecules in agarose gels is caused by their transient interactions (mainly hydrogen bonding) with the hydroxyl groups on the surface of agarose molecules and the decelerated collective mobility of hydrogen-bonded network of water molecules inside the pores. Previous NMR reports have detected small adsorption of anions (here, chloride ions) but not cations (here sodium ion) to agarose molecules inside gels [9]. Nevertheless, the altered dynamics of water molecules especially in the (first and second) solvation shell of sodium ions, is expected to perturb the mobility of sodium ions and the local electric field gradient they

experience. In line with this expectation, the translational diffusion coefficient of sodium ions decreased in agarose gels (Fig. 2), and the T_1- and especially T_2-Triple-Quantum-Filtered (TQF) data revealed the emergence of a new species of sodium ions in agarose gels within the slow-motion regime (Fig. 3). Through combination of single-quantum and triple-quantum ^{23}Na NMR relaxation data, we were able to identify three populations of sodium ions: (1) a population with bi-exponential relaxation roughly representing 30–40 % of total sodium ions. The population of this species showed little, if any, agarose concentration dependence, however both the T_1 (T_{1s} and T_{1l}) and T_2 (T_{2s} and T_{2l}) relaxation times of this species exhibited clear agarose concentration-dependent decreases (Fig. 5). The bi-exponential relaxation of this species indicates that the correlation time τ_c of fluctuations in the anisotropic quadrupolar interaction as the dominant ^{23}Na relaxation mechanism of sodium ions is slower than $1/\omega = 1.5ns$. This is consistent with a previously reported τ_c of 12 ns in 2.4 % agarose gel [11]. Due to the lack of accurate data on the quadrupolar coupling constant of (hydrated) sodium ions inside agarose gels at various concentrations, our data does not allow providing a reliable estimate of τ_c. (2) a major population with mono-exponential relaxation approximately amounting to 50–60 % of total sodium ions (shown in Fig. 5 in blue). This sodium ion species exhibits a concentration-dependent effect of agarose on T_1 and particularly T_2, with $T_2 \ll T_1$, suggesting a significant deviation from the fast extreme-narrowing regime which would otherwise implicate $T_2 \cong T_1$. The exact physical mechanism reconciling the mono-exponential relaxation behavior with $T_2 \ll T_1$ is unclear at this stage, but a similar effect was recently observed in other porous materials and attributed to anisotropic motions [12]. (3) a minor population with mono-exponential relaxation representing the remaining 10 % of total sodium ions (shown in Fig. 5 in red). This species is indistinguishable in T_1 relaxation from the previous species and in general is less affected by the presence of agarose gels than the other two species. Therefore, this species is more likely to be present in the center of pores where they can reside in the largest distance from agarose molecules. Nevertheless, they still experience an agarose concentration-dependent decrease in their T_1 and T_2, reflecting their increasingly decelerated motion. Besides, the T_2 of this sodium ion species is smaller than its T_1 at all the studied agarose gels, indicating a deviation from fast extreme-narrowing regime of motion. The deviation however seems not to be large enough to lead to an experimentally detectable bi-exponential relaxation. Further insight on the physical mechanisms behind the behavior of these three species of sodium ions, especially species 2, remains to be provided by future studies.

It is worth noting that there are several modes of motion, which modulate the anisotropic interaction between the electric quadrupole of ^{23}Na ions and the local electric field gradient (EFG) present at the site of ^{23}Na nuclei. The reorientational dynamics of hydrated ^{23}Na ions at pico-to-nanosecond timescale is one but not the only motion modulating this anisotropic interaction. Other modes of molecular motion could lead to EFG fluctuations and thereby modulate the quadrupolar interactions, e.g. motions of water molecules in the first and second hydration shells of sodium ions and the exchange of water molecules between hydration shells and bulk water or water near the surface of agarose gels can result in relaxation-active quadrupolar interactions. Interestingly, a recent study has shown quantitatively that the sub-picosecond EFG fluctuations associated to collective dynamics of water molecules and the associated solution structure relaxation underlies ^{23}Na NMR relaxation in electrolyte solutions in a broad range of temperatures and ion concentrations [31]. Another source of EFG fluctuations is the lateral and radial diffusion of sodium ions along or perpendicular to the surface of agarose chains, which provided that the correlation time of resultant EFG fluctuations is fast enough, can be ^{23}Na relaxation-active.

4.2. Potential applications of the combined single-quantum and TQF ^{23}Na NMR approach

Many cellular functions occur inside the crowded and often confined environment of membrane-less compartments formed through phase separation. Frequently, the multivalent electrostatic interactions, e.g. between negatively charged ribonucleic acids (RNAs) and positively charged fragments of protein, are the main driving force for the formation and stabilization of these compartments [3]. The presence of ions in these environments can alter the stability of these compartments and also influence the functional dynamics of biomolecules residing in them [4]. Considering that macromolecules occupy 10–40 % of total cellular volume (corresponding to a concentration of around 100–300 mg/mL), the upper limit concentration of 15 % agarose used in our study (corresponding to a concentration of 150 mg/mL) lies reasonably well within the range of crowdedness found inside cells [32]. The integrative ^{23}Na NMR approach presented here is a potentially powerful tool to monitor the dynamics of sodium and other biologically relevant spin-3/2 ions (like ^{35}Cl) inside biomolecular condensates and characterize their potential regulatory roles in health and particularly disease states. Another potential application as a complementary tool is in monitoring electrolyte dynamics, e.g. in relation with sodium ion battery development technologies [33].

5. Conclusion

To summarize, we have studied sodium ion dynamics inside agarose gels through ^{23}Na NMR relaxation. A new integrative approach is developed through combination of single- and triple-quantum ^{23}Na NMR relaxation data. Following this approach, we were able to disentangle the contribution of mono- and bi-exponential relaxing sodium ion species. Three populations of sodium ions were identified inside agarose gels, which their dynamics were differentially perturbed by agarose gels. Our study sheds light on the heterogeneity of sodium ion dynamics inside agarose gels and provides a new tool for monitoring dynamics of sodium and other spin-3/2 ions (e.g. chloride) in crowded, condensed or confined media.

Declaration of competing interest

The authors declare that they have no known competing financial interests or personal relationships that could have appeared to influence the work reported in this paper.

Data availability

Data will be made available on request.

Acknowledgements

This work is supported by a Deutsche Forschungsgemeinschaft (German Research Foundation, DFG) research grant (RE 3655/2-3) to N. R.-G. Prof. Christian Griesinger and Dr. Loren Andreas are acknowledged for useful discussions.

Appendix A. Supplementary data

Supplementary data to this article can be found online at https://doi.org/10.1016/j.ymeth.2024.05.015.

References

[1] S.F. Banani, H.O. Lee, A.A. Hyman, M.K. Rosen, Biomolecular condensates: organizers of cellular biochemistry, Nat. Rev. Mol. Cell Biol. 18 (2017) 285–298.
[2] S. Alberti, Phase separation in biology, Curr. Biol. 27 (2017) R1097–R1102.
[3] Y. Shin, C.P. Brangwynne, Liquid phase condensation in cell physiology and disease, Science 357 (2017) 357.

[4] Q. Chen, L. Zhao, A. Soman, A.Y. Arkhipova, J. Li, H. Li, Y. Chen, X. Shi, L. Nordenskiold, Chromatin Liquid-Liquid Phase Separation (LLPS) Is Regulated by Ionic Conditions and Fiber Length, Cells 11 (2022).
[5] J. Li, M. Zhang, W. Ma, B. Yang, H. Lu, F. Zhou, L. Zhang, Post-translational modifications in liquid-liquid phase separation: a comprehensive review, Mol. Biomed. 3 (2022) 13.
[6] J.R. Lewandowski, M.E. Halse, M. Blackledge, L. Emsley, Protein dynamics, Direct Observation of Hierarchical Protein Dynamics, Science 348 (2015) 578–581.
[7] L. Piculell, S. Nilsson, Anion-Specific Salt Effects in Aqueous Agarose Systems. 1. Effects on the Coil-Helix Transition and Gelation of Agarose, J. Phys. Chem. 93 (1989) 5596–5601.
[8] G. Madelin, J.S. Lee, R.R. Regatte, A. Jerschow, Sodium MRI: Methods and applications, Prog. Nucl. Magn. Reseon. Spectrosc. 79 (2014) 14–47.
[9] L. Piculell, S. Nilsson, Anion-Specific Salt Effects in Aqueous Agarose Systems. 2. Nuclear-Spin Relaxation of Ions in Agarose Gels and Solutions, J. Phys. Chem. 93 (1989) 5602–5611.
[10] J.C. Fuentes-Monteverde, S. Becker, N. Rezaei-Ghaleh, Biomolecular phase separation through the lens of sodium-23 NMR, Protein Sci. 30 (2021) 1315–1325.
[11] P. Lundberg, P.W. Kuchel, Diffusion of solutes in agarose and alginate gels: H-1 and Na-23 PFGSE and Na-23 TQF NMR studies, Magn. Reson. Med. 37 (1997) 44–52.
[12] E. Nimerovsky, New experimental observations of the behavior of sodium ions in saturated rock samples, J. Magn. Reson. 302 (2019) 72–87.
[13] N. Rezaei-Ghaleh, Water Dynamics in Highly Concentrated Salt Solutions: A Multi-Nuclear NMR Approach, ChemistryOpen 11 (2022) e202200080.
[14] X.A. Mao, J.X. Guo, C.H. Ye, Radiation Damping Effects on Spin-Lattice Relaxation-Time Measurements, Chem. Phys. Lett. 222 (1994) 417–421.
[15] N. Rezaei-Ghaleh, F. Munari, S. Becker, M. Assfalg, C. Griesinger, A facile oxygen-17 NMR method to determine effective viscosity in dilute, molecularly crowded and confined aqueous media, ChemCommun. (camb) 55 (2019) 12404–12407.
[16] A. Abragam, The Principle of Nuclear Magnetism, Oxford University Press, 1961.
[17] C.S. Johnson, Diffusion ordered nuclear magnetic resonance spectroscopy: principles and applications, Prog. Nucl. Magn. Reson. Spectrosc. 34 (1999) 203–256.
[18] R.L. Vold, J.S. Waugh, M.P. Klein, D.E. Phelps, Measurement of Spin Relaxation in Complex Systems, J. Chem. Phys. 48 (1968) 3831–3832.
[19] E.L. Hahn, Spin Echoes, Phys. Rev. 80 (1950) 580–594.
[20] G. Jaccard, S. Wimperis, G. Bodenhausen, Multiple-Quantum Nmr-Spectroscopy of S=3/2 Spins in Isotropic-Phase - a New Probe for Multiexponential Relaxation, J. Chem. Phys. 85 (1986) 6282–6293.
[21] C.W. Chung, S. Wimperis, Optimum Detection of Spin-3/2 Biexponential Relaxation Using Multiple-Quantum Filtration Techniques, J. Magn. Reson. 88 (1990) 440–447.
[22] J.R.C. Van der Maarel, Thermal relaxation and coherence dynamics of spin 3/2. I. Static and fluctuating quadrupolar interactions in the multipole basis, Concept. Magn. Reson. A 19a (2003) 97–116.
[23] A.G. Redfield, On the Theory of Relaxation Processes, IBM J. Res. Dev. 1 (1957) 19–31.
[24] P.D. Teal, C. Eccles, Adaptive truncation of matrix decompositions and efficient estimation of NMR relaxation distributions, Inverse Probl. 31 (2015) 045010.
[25] J. Ropp, C. Lawrence, T.C. Farrar, J.L. Skinner, Rotational motion in liquid water is anisotropic: A nuclear magnetic resonance and molecular dynamics simulation study, J. Am. Chem. Soc. 123 (2001) 8047–8052.
[26] I.P. Gerothanassis, Oxygen-17 NMR spectroscopy: basic principles and applications (part I), Prog. Nucl. Magn. Reson. Spectrosc. 56 (2010) 95–197.
[27] D. Lankhorst, J. Schriever, J.C. Leyte, Determination of the Rotational Correlation Time of Water by Proton Nmr Relaxation in H2o-O-17 and Some Related Results, Ber. Bunsenges. Phys. Chem. 86 (1982) 215–221.
[28] P.S. Hubbard, Nonexponential Nuclear Magnetic Relaxation by Quadrupole Interactions, J. Chem. Phys. 53 (1970) 985–987.
[29] W.S. Price, B.E. Chapman, P.W. Kuchel, Correlation of Viscosity and Conductance with Na-23+ Nmr T1 Measurements, Bull. Chem. Soc. Jpn. 63 (1990) 2961–2965.
[30] J. Kowalewsky, L. Maler, Nuclear Spin Relaxation in Liquids: Theory, Experiments, and Applications, CRC Press, 2017.
[31] I. Chubak, L. Alon, E.V. Silletta, G. Madelin, A. Jerschow, B. Rotenberg, Quadrupolar 23Na+ NMR relaxation as a probe of subpicosecond collective dynamics in aqueous electrolyte solutions, Nat. Commun. 14 (2023) 84.
[32] D. Collette, D. Dunlap, L. Finzi, Macromolecular Crowding and DNA: Bridging the Gap between In Vitro and In Vivo, Int. J. Mol. Sci. 24 (2023) 17502.
[33] J.Y. Hwang, S.T. Myung, Y.K. Sun, Sodium-ion batteries: present and future, Chem. Soc. Rev. 46 (2017) 3529–3614.